Methane Thiol SAMs Induce Reconstruction and Formation of Cu^+ on a Cu Catalyst under Electrochemical CO_2 Reduction

Go IIJIMA Hitoshi YAMAGUCHI Tomohiko INOMATA
Hiroaki YOTO Miho ITO Hideki MASUDA

特集

Cu electrode-based electrochemical CO_2 reduction using renewable energy is a promising method for conversion of CO_2 to useful compounds such as methane, ethylene and ethanol. Heteroatom-doped and/or -derived Cu as oxide-derived Cu have been investigated in context of development of a stable catalyst with high selectivity, whereas the role of heteroatoms is not yet well understood. It is not known whether heteroatoms act as a moiety of the catalyst or simply induce reconstruction of the catalyst. This work is an investigation of the role of the heteroatom in electrocatalytic CO_2 reduction with a Cu electrode modified with methane thiol monolayers (MT-Cu) which is able to distinguish the presence of heteroatom contamination originating from electrolyte or air. Controlled potential electrolysis of CO_2 using a MT-Cu electrode at −1.8 V at Ag/AgCl exhibits greater selectivity for C_2 products than an unmodified polycrystalline Cu electrode (bare Cu). On the other hand, a sulfur-modified Cu (S-Cu) electrode predominantly generates formate as a CO_2 reduction product. In an investigation of the mechanism, *in situ* attenuated total reflection surface-enhanced infrared absorption spectroscopy (*in situ* ATR-SEIRAS) is used as a powerful surface analyzer. Scanning electron microscopy (SEM) and X-ray spectroscopy (XPS) are also employed in the investigation. The spectroscopic data show that reconstruction and formation of Cu^+ on the Cu surface occurs at negative potential than − 1.4 V vs. Ag/AgCl by electrochemical reduction of methane thiol monolayers. DFT calculations are also performed under conditions close to the experimental conditions of electrical bias and aqueous electrolyte. The results indicate that a roughened surface is favorable for generating C_2 products. In addition, the Cu^+ moiety promotes generation of C_2 products, demonstrating that the doped heteroatom plays a crucial role in electrochemical CO_2 reduction.

Key words :
CO_2 reduction, Cu electrode, Methane thiol monolayers, Cu^+, C_2 products, Reconstruction, SEIRAS, Electrochemical catalysis, DFT calculation

Introduction

The conversion of CO_2 into valuable hydrocarbons is a crucial strategy for mitigating CO_2 emissions and exhaustion of fossil fuels[1)-3)]. Electrochemical CO_2 reduction is expected to be promising method because it uses renewable electricity from solar cells, wind-power generation or other green methods[4)-6)]. Among

the CO_2 reduction products, C_2 products such as ethylene and ethanol are used as inputs in production of fuels and commodity chemicals[7)-9)]. To promote conversion of CO_2 to C_2 products in electrochemical reactions, Cu catalysts with nano-structure[10)-15)], and Cu catalysts capable of controlling oxidation state (e.g. doping heteroatom)[16)-23)], and alloying[24)25)], have been researched. Among these catalysts, oxide-derived copper (OD-Cu), which was proposed by Kanan and co-workers[26)], is one of the most promising candidates. Other Cu catalysts induced by the presence of a heteroatom, such as nitride-derived copper (ND-Cu)[17)-19)], are also known to enhance electrochemical CO_2 reduction. The mechanism of enhancement in electrochemical CO_2 reduction employing OD-Cu has been proposed to originate from the oxidation state[27)-30)], the grain boundary[31)-33)] and defect sites[34)35)] on Cu. Although the attribution of the oxidation state of Cu, such as residual heteroatom-doped copper or cationic copper (Cu^+), has vigorously been studied[27)-30)], the investigations have been inconclusive because Cu is promptly oxidized upon exposure to air[32)]. The origin of the oxidation process is obscure. For this reason, *in situ* analyses, such as surface-enhanced Raman scattering (SERS) or X-ray adsorption spectroscopy (XAS), have been expected to be useful in elucidating the role of oxidation states of Cu. For example, Fu *et al*. performed *in situ* Raman spectroscopy, suggesting presence of Cu_2O on Cu nanocrystal which promoted C_2 products generation[36)]. Similarly, Lin *et al*. indicated persistent presence of Cu^+ on CuOx electrode under electrochemical CO_2 reduction by *in situ* XAS[37)]. However, analyses using these methods to date have not provided clarity. Mandal *et al*. previously reported that the oxidation state on Cu is not a factor enhancing CO_2 reduction on OD-Cu, since it is gradually diminished under electrochemical CO_2 reduction as estimated by *in situ* SERS measurement[32)]. However, this observation may be limited with respect to detection of small amounts of chemical species through electrolyte, although the method utilizing plasmon resonance has merit in enhancing the intensity in Raman scattering. Sufficiently oxidized Cu is also required for XAS measurements[28)]. For example, Scott *et al*. suggested absence of Cu^+ under electrochemical CO_2 reduction by *in situ* XAS measurements[38)]. Additionally, the interpretation of XAS data in evaluation of the oxidation state is challenging because it complicated by a mixture of various species[39)]. Development of other techniques is required to reveal the role of the oxidation state of Cu.

In this work, we employ self-assembled monolayers (SAMs) modified with methane thiol or sulfur as doped heteroatom on Cu (abbreviated as MT-Cu and S-Cu, respectively), to clarify the origin of the heteroatom. Controlled potential electrolysis (CPE) of CO_2 using the MT-Cu electrode demonstrates greater selectivity for C_2 products, which is similar to the selectivity promoted by the OD-Cu electrode. On the other hand, the S-Cu electrode generates formate as a CO_2 reduction product. The enhancement of CO_2 reduction on the MT-Cu electrode has also been evaluated employing not only a general surface analyzing technique, such as XPS or SEM, but also *in situ* ATR-SEIRAS measurements[40)]. The ATR-SEIRAS measurement provides the advantage of measuring *in situ* FT-IR without passing through electrolyte. Among other characteristics, CO_2 reduction on the MT-Cu electrode is promoted by a roughened Cu surface derived from electrochemical reduction of the methane thiol layer on Cu. ATR-SEIRAS measurements are unsuitable for detecting inorganic species such as oxidized Cu. However, we recognize that carbon monoxide (CO) as the intermediate of CO_2 reduction can function as a crucial marker for detecting the oxidation state on Cu, showing that the MT-Cu electrode has possessed Cu^+ character

even under reduction conditions. Through these investigations, we determined that the heteroatom on Cu induces reconstruction and formation of Cu^{+} on the Cu electrode.

Experimental Procedure

Materials

Materials for preparing Cu films, NH_4F (40 wt% in H_2O), $CuSO_4 \cdot 5H_2O$, Na_2EDTA, 2,2'-bipyridine, HCHO, and NaOH, were purchased from FUJIFILM Wako Pure Chemical.

Cu polycrystalline substrates for CPE were acquired from Nilaco Corporation. Cu monocrystalline substrates as Cu(111) and Cu(100) were purchased from Mateck. Dimethyl disulfide used for preparation of the methane thiol monolayer on the Cu substrate was purchased from Tokyo Chemical Industry Co., Ltd.

The other compounds used in electrolysis, including CO_2 and $NaHCO_3$, were obtained from Taiyo Nissan and FUJIFILM Wako Pure Chemical, respectively.

Apparatus

Fourier transform infrared (FT-IR) and attenuated total reflection spectra were measured using a JASCO FT/IR-4200 and a JASCO ATR PRO410-S spectrometers. Gas-chromatography mass spectra (GC-MS) were measured using a JEOL JMS-Q1050GC instrument with an Inert Cap FFAP column. Gas chromatography (GC) with a flame ionization detector were performed using a Shimadzu GC-2014 instrument with an Agilent Inc. B-WAXETR column. GC measurements with a thermal conductivity detector were performed using an Agilent Technologies 7890A instrument with an Agilent Inc. TC-Molsieve 5A column. Ionic chromatography was carried out using a Shimadzu Prominence Ion Chromatograph System with a Shim-pack IC-SA3 column. X-Ray photoelectron spectra (XPS) and Auger spectra were taken using an ULVAC-PHI XPS PHI5000 system with Al Kα radiation. X-ray diffraction (XRD) was recorded with a Rigaku SmartLab system at 298K using Cu Kα radiation. Scanning electron microscopy (SEM) was measured using a Hitachi High-Technologies SEM S-5500 operated at back scattered detector mode (10 μA and 1.5 kV). The sample was mounted with double-sided carbon tape. Thermal desorption spectra (TDS) were obtained using an ESCO WA1000S/W system operated at temperatures from 50 to 350 °C at a programmed rate of 30 °C/min.

Preparation of Cu electrodes for CPE

Cu samples were prepared from polycrystalline Cu foil (Nilaco, 99.9999 %) with a thickness of 0.1 mm. The Cu electrode modified with methane thiol monolayer, abbreviated as MT-Cu, was prepared according to the previously established procedure[41)42)]. The Cu electrodes were washed with 1.0 M HCl aqueous solution and then cleaned with Milli-Q water using an ultrasonicator for 30 minutes. The MT-Cu electrode was prepared by direct casting of dimethyl disulfide solution diluted by EtOH onto the Cu electrode via addition of a few drops over the course of a few days. After washing with EtOH and $CHCl_3$, MT-Cu was obtained. The preparation of MT-Cu was confirmed by XPS. Sulfur-doped Cu, abbreviated as S-Cu, was prepared as described previously[21)]. Sulfur was electrochemically deposited onto the polished Cu substrate using square wave voltammetry with a forward potential of –1.16 V vs. Ag/AgCl for 10 ms and a reverse potential of –0.41 V for 20 ms in plating solution (4 mM $CuSO_4 \cdot 5H_2O$, 4 mM thiourea, and 0.648 M HCl). The electrochemical deposition was completed in 60 seconds. Monocrystalline Cu substrates were prepared by electropolishing and rinsing with diluted acid as previously reported[43)].

特集

The modification of methane thiol monolayer on monocrystalline Cu was carried out using the same procedure used for preparation of polycrystalline Cu. Anodized Cu electrodes were obtained by improving the previously reported method[44]. Cu foil was electrochemically oxidized in 3 M NaOH aqueous electrolyte in the constant current condition (10 mA/cm^2) for 60 seconds to form $Cu(OH)_2$ nanowire arrays. Reductively anodized Cu was prepared by reducing anodized Cu in 1.0 M HCl aqueous solution, and characterized by XPS and SEM measurements.

Preparation of Cu film for SEIRAS measurement

The fabrication of Cu films was performed in accordance with previous studies[30)45)]. The Si ATR hemispherical prism prepared for the SEIRAS measurements (0.98 inch diameter, manufactured by Pier Optics Co., Ltd.) was polished with 0.05 mmφ alumina for about 10 minutes and then washed in Milli-Q water using an ultrasonicator for 30 min. The surface of the Si prism was etched with a 40% NH_4F solution, washed with Milli-Q water and continuously plated with 0.25 M HCHO, 0.02 M $CuSO_4$, 20 mM Na_2EDTA, and 0.3 mM 2,2-bipyridine; T = 75 – 80 °C for 1.0 min. After the deposition, the resistance of the film surface was measured to be 10 – 30 ohms. The resulting Cu films were washed with Milli-Q water, assembled into an electrolysis cell, and blanketed with 0.1 M $NaHCO_3$ aqueous solution saturated with Ar. The films were then washed by performing 15 cycles of cyclic voltammetry (CVs from –0.13 to –0.7 V vs. Ag/AgCl at a scan rate of 0.05 Vs^{-1}). MT-Cu films for SEIRAS measurements were prepared using plated Cu film as substrate. The modification of methane thiol onto the Cu film was performed according to the same procedure used to prepare the MT-Cu electrode for CPE. After the modification, the MT-Cu film was cleaned by performing 15 cycles of CVs in the same potential range used in the cleaning step.

Electrochemistry

Electrochemical measurements were performed using a BAS ALS model 660E analyzer. CV was performed using one of the Cu electrodes as the working electrode, carbon paper as the counter electrode and Ag/AgCl (3 M NaCl) as the reference electrode. The reference electrode was formed of two layers of glass tube to prevent contamination of Ag against electrolyte or other electrodes. A 0.1 M $NaHCO_3$ aqueous solution was prepared as the electrolyte.

Controlled potential electrolysis of CO_2 using Cu electrodes

The reduction reaction was performed using Milli-Q water containing 0.1 M $NaHCO_3$. Carbon paper and Cu, MT-Cu, or S-Cu plate were used as the counter and working electrodes, respectively. The potentials of the working electrode were –1.2, –1.4, –1.6, and –1.8 V vs. Ag/AgCl, and the reaction time was 1.0 hr. Analysis of the products of electrolysis showed that formate was detected by ion chromatography, ethanol was inferred by gas chromatography (Shimadzu GC-2014), and other gaseous products were detected by gas chromatography (Agilent Technologies 7890A), respectively.

Measurements of *in situ* ATR-SEIRAS

Potential- and time-dependent *in situ* ATR-SEIRAS measurements of the samples were performed using Cu film that was plated on a hemispherical Si ATR prism by the previously reported procedure[30)40)]. Spectra were recorded in the Kretschmann attenuated total reflection (ATR) configuration using a JASCO FT/IR4200 spectrometer equipped with a HgCdTe (MCT) detector. Electrochemical measurements were performed by a BAS ALS600 series electrochemical analyzer using Cu films as the working electrode,

carbon paper as the counter electrode and Ag/AgCl (3 M NaCl) as the reference electrode. A 0.1 M $NaHCO_3$ aqueous solution was used as the electrolyte that was saturated with either Ar or CO_2. These films were characterized and measured at least three times to confirm their reproducibility.

DFT calculations

To evaluate the reaction behavior at the Cu electrode, density functional theory (DFT) calculations were performed using the Quantum-Espresso (Open-Source Package for Research in Electronic Structure, Simulation, and Optimization)[46]. This program was embedded with the Effective Screening Medium method (ESM)[47)48)] to calculate the external electric field or the bias potential, and also with the Reference Interaction Site Model (RISM)[49)] to evaluate the distribution of solvent, solute and their potentials[50)51)]. In the Quantum-Espresso, we used the generalized gradient approximation (GGA) parameterized by Perdew-Burke-Ernzerhof (PBE) functionals. The projector augmented wave (PAW) method was employed and the kinetic cutoff energies for the wavefunctions and the charge density of plane wave were 540 eV and 4000 eV, respectively. The crystalline facets of pristine copper, (111), (100), (110), and (211), were approximated by a 3 × 3 × 3 slab in a 30 Å vacuum. Two lower layers of the supercell were fixed and one upper layer was allowed to move freely due to the interaction with adsorbates. The smearing parameter of 0.54 eV using the Gaussian method was applied. The reciprocal space was sampled with 8 × 8 × 1 Monkhorst-Pack mesh. The self-consistent field (SCF) tolerance was set to 1×10^{-8} eV/atom. Adsorbates and the surface of Cu atoms were optimized until the magnitude of residual forces was below 0.0005 eV/Å.

Results and Discussion

Preparation and characterization of MT-Cu electrode

The modifications of methane thiol on polycrystalline Cu, Cu(111) and Cu(100) were evaluated by XPS analysis, which showed a peak ascribed to S_{2p} at approximately 163 eV (Fig. 1). Other than the peak ascribed to S_{2p}, the peak ascribed to Cu_{2P} was also observed as similar binding energy on each electrode. The modification of methane thiol on Cu was also confirmed by *in situ* ATR-SEIRAS measurements, which is described in the section "Surface analysis of each electrode before/after electrolysis", in detail.

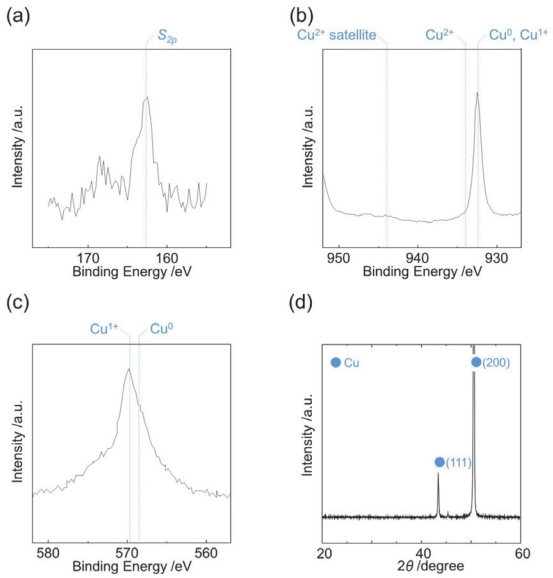

Fig. 1 Characterization of MT-Cu for CPE. (a) XPS (high-resolution S_{2p} spectrum), (b) XPS (high-resolution Cu_{2p} spectrum), (c) Cu LMM Auger spectrum, and (d) XRD

Controlled potential electrolysis

CPE was performed using each electrode at −1.2, −1.4, −1.6, and −1.8 V vs. Ag/AgCl. The results are shown in Fig. 2. A comparison of polycrystalline Cu with/without methane thiol monolayers and sulfur-doped Cu, which are abbreviated as MT-Cu, bare Cu, and S-Cu, indicated that the products of CO_2 reduction were are significantly different. When using

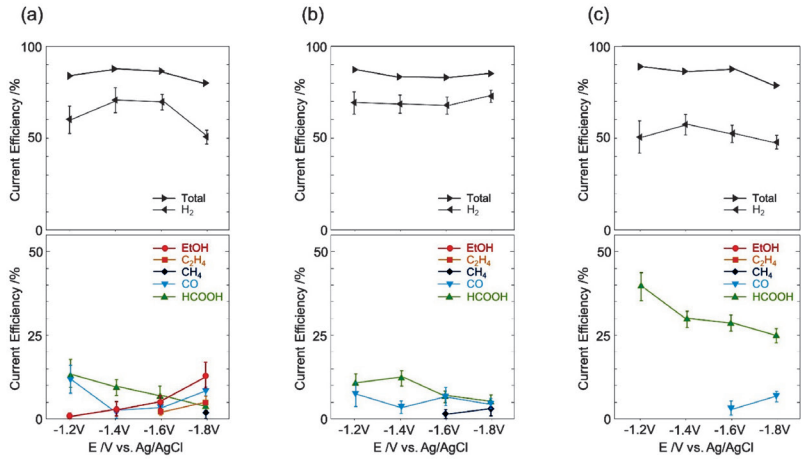

Fig. 2 Products obtained from electrochemical CO_2 reduction using Cu electrodes and their current efficiencies (%). (a) MT-Cu, (b) bare Cu and (c) S-Cu electrodes

bare Cu electrode, carbon monoxide and formate were mainly produced and methane was also detected. On the other hand, greater amounts of methane, ethylene, and ethanol were generated when using the MT-Cu electrode at each of potentials. In particular, it was found that C_2 products such as ethylene and ethanol are produced in greater amounts than C_1 products such as methane. This result is very interesting in context of using a sulfur-doped Cu electrode, because previous investigations have shown that formate is the main product generated using a S-Cu electrode[20-23]. The difference between our present observations and the results of previous investigations[20-23] is believed to be due to the difference in the sulfur groups with/without methyl substitution which affect the electrochemical reduction pathways from CO_2 to its reduction products. García-Muelas *et al.* previously proposed that sulfur was likely to adsorb protons and act as proton donor for CO_2 to generate formate[20]. Even if this does not occur, sulfur would promote bidentate adsorption of CO_2. This manner of adsorption was previously reported in formation of the first intermediate during generation of formate from CO_2 [21]. Similar performance of a sulfur-doped Cu electrode without methyl substitution was also confirmed in our experiment using the S-Cu electrode, which is shown in Fig. 2(c).

In order to elucidate the behavior of the MT-Cu electrode, monocrystalline Cu substrates such as Cu(111) and Cu(100) were also applied as electrodes for CPE. Methane and ethylene were produced from monocrystalline Cu at −1.8 V vs. Ag/AgCl. Furthermore, specific enhancements in production of hydrocarbons and alcohols were not observed when the MT-Cu electrode was used. This observation differs from the results of CPE experiments using the polycrystalline Cu electrode modified with methane thiol. XPS analysis before CPE showed that the amount of methane thiol on monocrystalline Cu electrodes was less than the amount on the polycrystalline Cu electrode, suggesting that the effect of the methane thiol monolayer is limited for each monocrystalline Cu.

Surface analysis of each electrode before/after electrolysis

(i) Durability of MT-Cu

The durability of the methane thiol monolayer on the MT-Cu electrode was also evaluated using XPS which is a highly sensitive surface analysis method (Fig. 3). After CPE using the MT-Cu electrode at each potential, XPS showed that a peak at 163 eV, which is ascribed to S_{2p} of methane thiol, disappears at a negative potential greater than −1.4 V, as shown

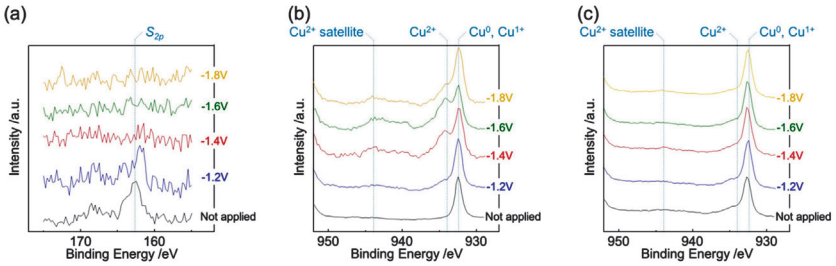

Fig. 3 XPS analyses of Cu electrodes before CPE (black) and after CPE at −1.2 (blue), −1.4 (red), −1.6 (green), and −1.8 V (yellow). (a) High-resolution S_{2p} spectra of MT-Cu, (b) high-resolution Cu_{2p} spectra of MT-Cu and (c) high-resolution Cu_{2p} spectra of bare Cu

in Fig. 3(a). From these results, the contribution of methane thiol in CO_2 reduction should be considered only at low negative potential. Therefore, the enhancement in hydrocarbon generation at high potential was deduced to be attributed to other factors. The other notable observation in the XPS analysis suggests that an oxidized layer is formed after CPE using the MT-Cu electrode, whereas the metallic Cu phase remains consistent when the bare Cu electrode is used. The formation of the oxidized layer on MT-Cu(111) after CPE was also observed by GIWAXS analysis, which will be discussed in more detail below.

(ii) Contribution of the surface state in enhancement of hydrocarbon generation

The contributions of the chemical environment, morphology, and/or gradient pH on the electrode surface to hydrocarbon generation were evaluated using surface analysis, which was performed using XPS, GIWAXS, SEM, and *in situ* ATR-SEIRAS measurements. As mentioned above, XPS analysis and *in situ* ATR-SEIRAS measurements showed a change in the chemical state of MT-Cu, indicating that the methane thiol layer is removed at high negative potential. It is assumed that so-called reductive desorption causes the monolayers to be electrochemically desorbed from the substrate[41)52)]. Instead, the methane thiol layer on the Cu substrate was replaced by an oxidized phase, which is more likely to be generated at potentials higher than −1.4 V, representing a range of potentials where the methane thiol layer will be desorbed (Fig. 3(b)). On the other hand, the oxidized phase was not observed when using bare Cu electrode at each of the potentials examined (Fig. 3(c)). This indicates that the formation of oxidized phase might be a key step in characterizing the catalytic behavior of the MT-Cu electrode. We also carried out SEM analysis for these electrodes, which showed morphological changes occurring on each electrode (Fig. 4). However, the morphological change occurring on the MT-Cu electrode appeared to be more extreme than the change occurring on the bare Cu electrode. Summarizing the results obtained so far, at higher negative potential than −1.4 V, electrochemical CO_2 reduction is not promoted by chemical species such as methane thiol but is instead promoted by other factors such as morphology and/or gradient pH on the surface of the electrode. The facet analyses of MT-Cu electrodes before/after CPE were also performed using electrochemical OH anion deposition which was previously reported by Raciti *et al* [53)]. In the analysis, we used the MT-Cu electrode as well as Cu substrates such as Cu(111), Cu(100), polycrystalline Cu, anodized Cu, and reductively anodized Cu electrodes to make comparisons. The results shown in Fig. 5, which indicates that the current peak ascribed to the OH anion adsorbed on the MT-Cu electrode before CPE is at −0.40 V. In addition, measurements using the MT-Cu electrode after CPE have two current peaks at −0.41 and

特集

−0.44 V, which are higher negative potentials than the potentials observed before CPE. The adsorption potentials of OH anion measured using Cu(111), Cu(100), and polycrystalline Cu electrodes are −0.41, −0.44, and −0.43, respectively. From these results, the MT-Cu electrode before CPE appears to have the same facet as Cu(111). However, the interpretation that the MT-Cu electrode has the same facet as Cu(111) was erroneous because these measurements were supposed to have been performed against unmodified substrates. Therefore, considering the effect of the modified Cu electrode, the potential shift observed before/after

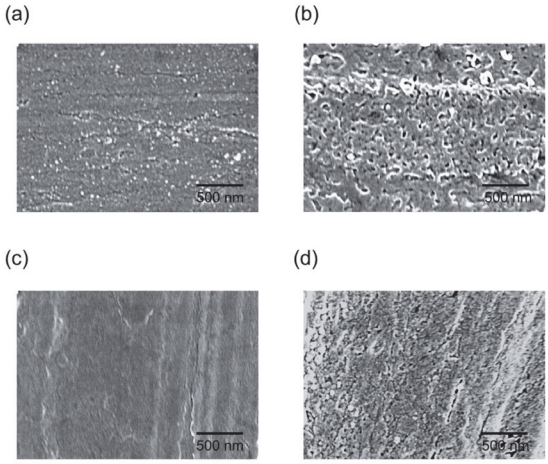

Fig. 4 SEM images of (a) the MT-Cu electrode before CPE, (b) the MT-Cu electrode after CPE, (c) the bare Cu electrode before CPE, and (d) the bare Cu electrode after CPE

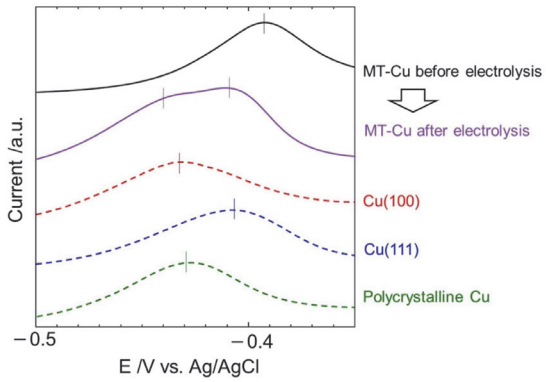

Fig. 5 Facet analyses employing linear sweep voltammograms recorded in 10 mV/s in 1 M KOH aqueous solution for the different types of Cu electrodes, MT-Cu before CPE (black), MT-Cu after CPE (purple), Cu(100) (red dash), Cu(111) (blue dash), and polycrystalline Cu (green dash)

CPE using the MT-Cu electrode appears to be due to inhibition of OH anion adsorption by the methane thiol monolayer. The results of adsorption experiments considering the effect of OH anion after CPE using the MT-Cu electrode indicate two current peaks at different potentials with one detected at greater negative potential than the analogous peak observed when the polycrystalline Cu electrode was used. Raciti *et al.* previously reported that the roughened Cu electrode with Cu(211) was likely to adsorb OH anion at greater negative potential than other facets such as Cu(111) and Cu(100)[53]. This indicates that the current peak at negative potential observed after CPE using MT-Cu was due to a more roughened surface than the surface of the polycrystalline Cu electrode.
Taken consideration about reductive desorption of sulfur on Cu electrode, the results of CPE using S-Cu electrode are seemed to be similar to that of MT-Cu electrode, however, they were different from each other.

We performed *in situ* ATR-SEIRAS measurements to probe the chemical state of CO which is an intermediate in reduction of CO_2. The *in situ* ATR-SEIRAS measurements have been performed employing some Cu films and/or electrolyte by other groups, and they indicated various features in electrochemical CO_2 reduction[30)45)54)-57)]. For example, Malkani *et al.* studied *in situ* ATR-SEIRAS measurements employing OD-Cu film, and showed the shift of CO peak to lower frequency due to reconstruction of Cu film[55)]. Besides, Ayemoba *et al.* suggested the affection of cationic electrolyte by change of electrolyte[57)]. From the merit in this measurement method, such as high sensitivity against electrode surface, we performed to elucidate the property of MT-Cu electrode under electrolysis. The Cu film for the ATR-SEIRAS measurement was prepared according to our previously reported method

[30]. We confirmed the oxidized phase on Cu film which was plated by a non-electrochemical procedure. The oxidized phase was electrochemically removed by cyclic voltammetry in the range of −0.13 ~ −0.7 V vs. Ag/AgCl. In preparation of methane thiol-modified Cu film for ATR-SEIRAS, (abbreviated as MT-Cu film), the electrochemical polishes were performed twice, before and after methane thiol modification.

We carried out time dependent *in situ* ATR-SEIRAS measurements with CPE at −1.2, −1.4 and −1.6 V to investigate the potential and time dependence under electrochemical CO_2 reduction. One of the merits of using this method is to generate greater resolution of the observed peaks in comparison with potential dependent *in situ* ATR-SEIRAS measurements. The results obtained from the ATR-SEIRAS measurements using MT-Cu and bare Cu films are shown in Fig. 6. These results indicate some spectral differences. At the potential of −1.2 V the peak between 2000 and 2100 cm^{-1}, ascribed to CO [30)45)54)-57)], was observed for both of the films but the peak shapes are different from each other. The peak top was observed at 2020 cm^{-1} for the MT-Cu film and at 2060 cm^{-1} for the bare Cu film. This difference is assumed to originate from factors such as the site of adsorption of CO and effects resulting from other chemical species, the applied potential and other possible effects. The peak detected at 2060 cm^{-1} is ascribed to CO adsorbed at the atop site of Cu, as previously reported[45)54-57)].We previously attempted to identify the origin of the peak at 2020 cm^{-1} using Cu films which have altered oxidation states on the Cu surfaces [30)]. It was concluded that the shift of the CO peak to a lower frequency region in accordance with an increase in the oxidation state of $Cu(OH)_2$ was due to an interaction between the CO and OH moieties adsorbed on the surface of the Cu film. The observation of the peak shift in the ATR-SEIRAS measurement using the MT-Cu film was similarly inferred as a result of interactions of CO with other species at −1.2 V. Additionally, the interaction between CO and sulfur was studied by other groups using DFT calculations, with results indicating that subsurface sulfur promotes adsorption of CO and H on the Cu surface [58)]. From these results, we assigned the peak observed at 2020 cm^{-1} to CO adjacent to methane thiol. However, the peak shift trend of this

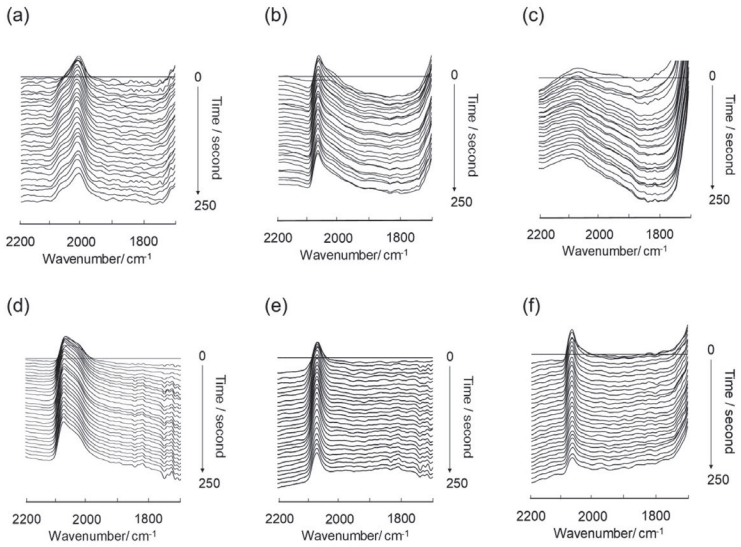

Fig. 6 Time dependent *in situ* ATR-SEIRAS using Cu films under CO_2. The spectra using MT-Cu film were measured at (a) −1.2 , (b) −1.4 and (c) −1.6 V vs. Ag/AgCl. The spectra using bare Cu film were measured at (d) −1.2, (e) −1.4 and (f) −1.6 V vs. Ag/AgCl, respectively. The spectrum (d) using bare Cu film at −1.2 V was reported in our previous work[30)]

chemical interaction is altered at other potentials relative to −1.2 V. At a higher negative potential (−1.6 V), the peak detected in the ATR-SEIRAS measurement using the MT-Cu film becomes wider than the peak detected at −1.2 V. On the other hand, the peak observed in the measurement using bare Cu film at −1.6 V is narrower than the peak detected using MT-Cu, which was detected at 2060 cm^{-1}. This latter peak is ascribed to CO adsorbed to the atop site on metallic Cu. The wide peak observed using the MT-Cu film was attributed to factors other than the chemical interaction between CO and sulfur, because the methane thiol layer had been removed from the surface at −1.6 V, as shown in Fig. 3(a). Gunathunge *et al.* previously reported that the peak observed in the low frequency region is ascribed to CO adsorbed on Cu(100) in the presence of strong coupling with another CO molecule [56]. In our previous work, we also suggested that the peak detected in low frequency region has a similar origin[30]. From this viewpoint, the peak observed below 2020 cm^{-1} is assigned to CO adsorbed on Cu in the presence of coupling with another CO molecule. The peak detected near 2100 cm^{-1} was previously ascribed to CO on Cu^{+}[55]. Another possibility is H adsorbed on Cu [54]. As mentioned above, the sulfur on Cu was believed to promote H adsorption[58]. However, it is difficult to determine whether or not the peak observed near 2100 cm^{-1} arises from adsorbed H, because the methane thiol layer was removed from surface at negative potential greater than −1.4 V. Therefore, we assign this peak (at −1.6 V) observed in the high frequency region to the CO adsorbed on Cu^{+}, as discussed in more detail below. The wide peak observed at −1.6 V using MT-Cu film indicates that CO is adsorbed at multiple sites of Cu to generate an arrangement which includes CO on Cu^{+} (observed in the high frequency region), CO at the atop site of Cu (observed at 2060 cm^{-1}), and CO on Cu in the presence of strong coupling with other CO molecules and/or OH ions (observed in the low frequency region).

DFT calculations for insight of CO_2 reduction on Cu electrode

Electrochemical CO_2 reduction at a negative potential greater than −1.4 V using the MT-Cu electrode promotes conversion of CO_2 to hydrocarbons with particular enhancement of generation of C_2 species. This is attributed to a morphological effect and formation of Cu^{+} on the Cu surface. The morphological effect on Cu had been considered as a main factor involved in generation of C_2 compounds, as reported by other research groups[10)-12)14)]. In order to elucidate the mechanism for electrochemical CO_2 reduction on the roughened Cu electrode, we carried out DFT calculations in combination with an implicit solvation method known as the reference site interaction model (RISM)[49]. Furthermore, we applied an effective screening medium (ESM) in the DFT calculations[47)48)], which enabled us to simulate the electrochemical interface[50)51)]. In the calculations, we evaluated C_2 formation on several facets of Cu to clarify the effects of surface morphology and protons from H_2O. Previously, C_2 formation pathways including CO-CO dimerization, a COH-CO reaction

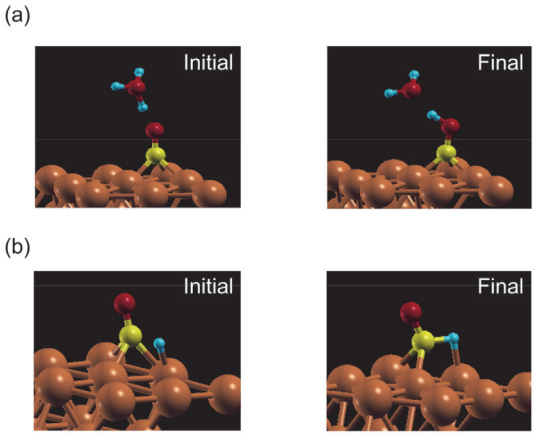

Fig. 7 Representative reaction behaviors (a) between CO and H_3O^{+} in the initial and final states and (b) between CO and adsorbed H in the initial and final states on Cu(111)

and a CHO-CO reaction, were proposed[59)-62)]. Therefore, we first investigated protonation of CO to COH or CHO (Fig. 7). In considering protonation of CO, our calculation indicated that both pathways depend on the positions of protons which would react with CO. We calculated protonation to CO at −1.4 V vs. SHE (which is believed to be equivalent to −1.6 V vs. Ag/AgCl under experimental conditions) on the Cu(111) electrode in 0.1 M Na_2SO_4 aqueous solution. The calculations showed that generation of COH is favored when CO reacts with a proton of a hydronium cation accompanied by an electron in an Eley-Rideal reaction[63)]. On the other hand, CHO is also produced in a reaction of CO with adsorbed H, which follows proton reduction by an electron in a Langmuir-Hinshelwood reaction[63)]. We concluded from these calculation results that reactants such as CO, COH or CHO for C_2 formation could be employed in our model. Next, we investigated C_2 formation on Cu(111) by three pathways, as outlined above and described in Fig. 8(a) and Fig. 9. The results indicate that CO-CO dimerization does not occur, while the CO-CHO and CO-COH reactions proceed. CO-CO dimerization is not favorable because two CO intermediates have the same charge distribution, resulting in repulsion between two CO molecules. The repulsion of two CO intermediates was also observed for the Cu(100) surface, which was previously reported as a favorable facet to produce C_2 products [43)56)], as shown in Fig. 8(b). On the other hand, the calculation for the reaction of CO with COH or CHO on Cu(111) shows that both pathways proceed by employing CO located at the atop site of Cu. However, the CPE data obtained using the Cu(111) electrode revealed that production of ethylene as a C_2 product is comparable to production of methane. In other words, the C_2 formation pathways employing COH or CHO compete with the methane production pathway. It is believed that the CO-

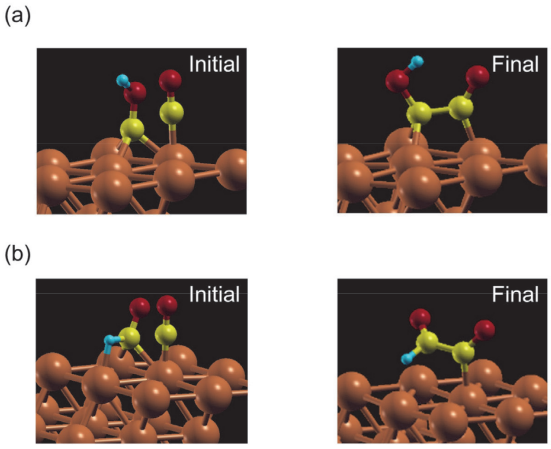

Fig. 9 Representative reaction behaviors (a) between CO and COH in the initial and final states and (b) between CO and CHO in the initial and final states on Cu(111)

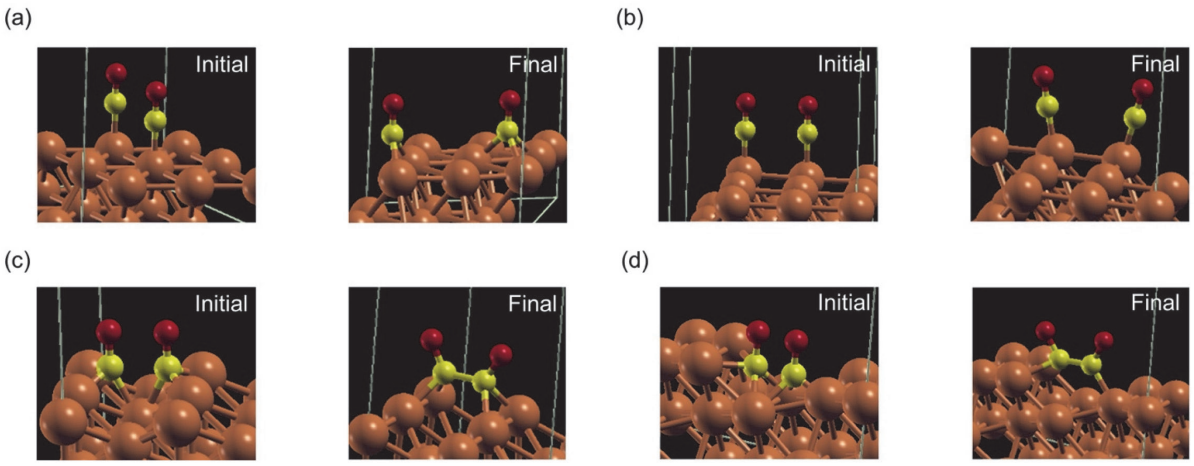

Fig. 8 Representative behaviors of CO-CO dimerization (a) in the initial and final states on Cu(111), (b) in the initial and final states on Cu(100), (c) in the initial and final states on Cu(110), and (d) in the initial and final states on Cu(211)

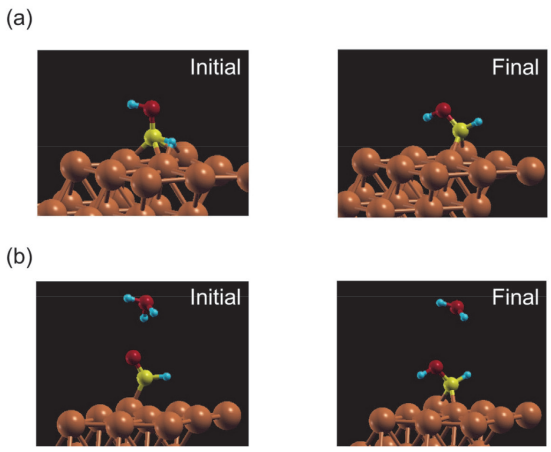

Fig. 10 Representative reaction behaviors (a) between COH and adsorbed H in the initial and final states and (b) between CHO and H_3O^+ in the initial and final states on Cu(111)

COH and CO-CHO reactions are limited because the reaction of CO with protonated CO proceeds only when they are located at adjacent position on Cu. As mentioned above, two adjacent CO moieties will likely repulse each other, indicating that combination of adjacent CO and protonated CO does not occur to a significant extent. Alternatively, protonated CO (COH or CHO) is likely to be converted to methane. Conversion to CHOH as an intermediate for methane formation from COH or CHO was confirmed by DFT calculations as well [64], as shown in Fig. 10. On the basis of the calculation results indicating that C_2 formation on Cu(111) and Cu(100) is unfavorable, we also evaluated the Cu(110) facet and the Cu(211) facet for calculation of C_2 formation. As shown in the XRD analysis (Fig. 1(d)), C_2 formation on Cu(211) was not observed. However, we investigated this facet to evaluate the effect of morphology on Cu as a roughened surface. The calculated results are shown in Fig. 8(c) and Fig. 8(d), which indicate that CO-CO dimerization proceeds on both the Cu(110) surface and the Cu(211) surface without repulsion of the two CO moieties. The results indicate that a roughened surface is preferable for promotion of C_2 production from CO directly. As outlined above, the Cu films investigated in the ATR-SEIRAS measurements and the polycrystalline Cu for the CPE measurements have a roughened surface as confirmed by OH anion adsorption experiments (Fig. 5). However, in spite of polycrystalline Cu possessing a roughened surface, production of C_2 compounds was less effective than the production measured using the MT-Cu electrode. The difference between the experimental data and the DFT calculations is due to fewer active sites being available on the polycrystalline Cu electrode used for CPE. The roughened surface in the nanometer scale, as described in DFT calculations, does not exist on the polycrystalline Cu electrode. On the other hand, the roughened surface in the nanometer scale using the MT-Cu electrode was confirmed by SEM spectroscopy, as shown in Fig. 4(b), indicating that the MT-Cu electrode under CPE has favorable facets to promote generation of C_2 compounds derived from reductive desorption of the methane thiol layer from Cu at high negative potential. The formation of the roughened surface on Cu was similarly reported by other groups using an oxygen- or nitrogen-containing Cu electrode[18)32)33)], revealing that reductive desorption of the heteroatoms in Cu induce morphological changes in the nanometer scale. It was also claimed that production of C_2 products such as ethylene or ethanol are increased by the roughened morphology of Cu.

Mechanism of electrochemical CO_2 reduction employing MT-Cu

From the investigation using spectroscopic analysis and DFT calculations, we proposed that the mechanism for generating C_2 compounds such as ethylene and ethanol can be explained in terms of the nanoscale morphological effect of the reconstructed Cu surface induced by reductive desorption of the methane thiol layer from Cu at negative potentials greater than −1.4 V. We assumed that there is another effect involved in promotion of C_2 product

generation. The ATR-SEIRAS measurements and XPS spectroscopy after CPE, provided data which led us to postulate that Cu^+ is formed under CPE, which promotes CO-CO dimerization. Xiao *et al.* previously reported that the combination of Cu^+ and Cu^0 phases promotes generation of both C_1 and C_2 products from CO_2 on the basis of DFT calculations, while the Cu electrode, which has only Cu^0, does not promote C_2 formation[65]. However, the presence of Cu^+ has been discussed[27)-30)], because a method for detecting it *in situ* has not been established. *In situ* Raman spectroscopy, which has high sensitivity for analysis of inorganic surfaces, is expected to overcome this problem. However, detection of Cu oxides such as Cu^+ and Cu^{2+} under CPE has not yet been successful[32]. XAS has also been employed for observations of Cu oxide under CPE[28], and the existence of Cu oxide in this context is being debated. The difficulty in the Cu oxide analysis is in detecting trace amounts of Cu oxide in a Cu electrode under reductive conditions. This has made direct observation of very small amounts of Cu oxide essentially impossible thus far. One way around this problem is to use a marker species. In our experiments using *in situ* ATR-SEIRAS spectroscopy, CO was adopted as an observable species to evaluate CO_2 reduction. The peak ascribed to CO is likely to shift as a result of the effects of the presence of metals or adsorption sites on the metals, as reported previously[30)45)54)-57)]. As mentioned above, Malkani *et al.* ascribed the peak at 2100 cm^{-1} to CO adsorbed on Cu^+ [55], which was also detected in our measurement using MT-Cu film. Furthermore, our XPS analysis after CPE using MT-Cu showed that Cu oxide is generated. This indicates that Cu^+ or Cu^{2+} is formed under electrolysis and is immediately combined with O_2 after exposure of the electrode to air. From these observations, the peak at 2100 cm^{-1} was assigned to CO on Cu^+, and it could be affirmed that CO plays a crucial role as a marker for investigating the inorganic electrode. The peak of CO on Cu^+ in the high frequency region and the peak of CO-CO coupling in the low frequency were spontaneously detected in the ATR-SEIRAS measurements. This suggests that the combination of the Cu^+ and Cu^0

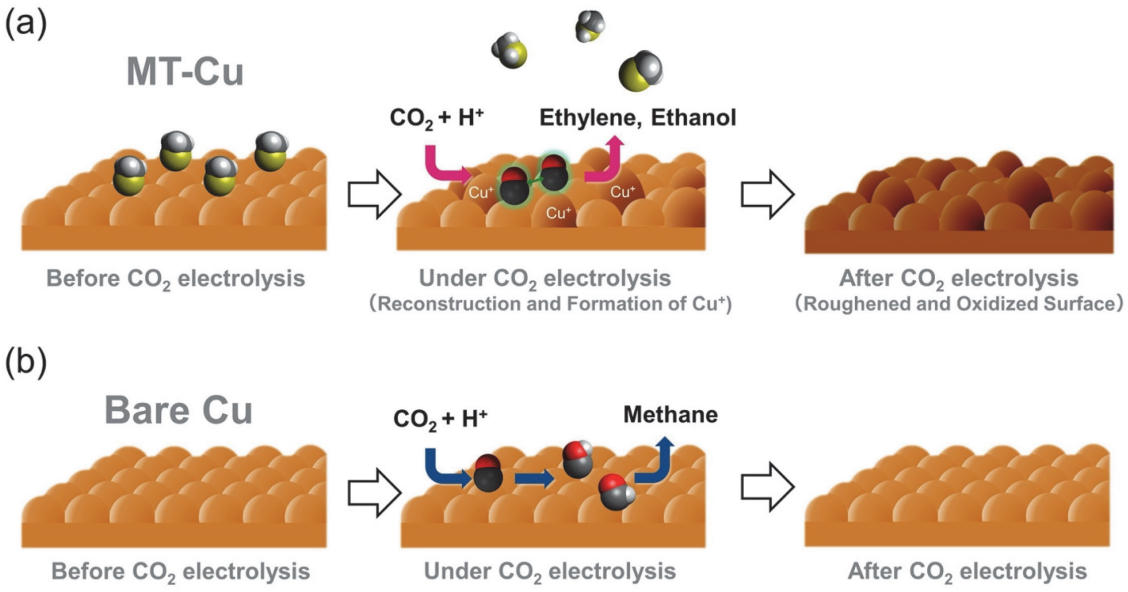

Scheme 1 Schematic illustrations of possible reactions on the Cu electrodes. (a) Showing reactions on the MT-Cu electrode as follows; (i) formation of methane thiol monolayer on Cu, (ii) reductive desorption of methane thiol monolayer inducing reconstruction and formation of Cu^+ on the Cu surface, which promote CO_2 reduction for generation of C_2 products through CO-CO dimerization, and (iii) formation of oxidized Cu after CPE. (b) Showing the reaction for generation of methane through a COH or a CHO intermediate on a bare Cu electrode

phases promotes CO-CO dimerization, as reported in the previous work [65]. Considering all of the above, the mechanism of electrochemical CO_2 reduction using MT-Cu is explained as follows (Scheme 1). 1) Before CPE, methane thiol layer is formed on the Cu substrate as SAMs. 2) The methane thiol layer on the MT-Cu electrode is desorbed under CPE which is performed at a greater negative potential than −1.4 V vs. Ag/AgCl. Reductive desorption of methane thiol induces not only a morphological change at the nanometer scale but also formation of Cu^+ on the Cu surface. The roughened and/or cationic Cu electrode causes an increase in the likelihood that two CO molecules will dimerize prior to protonation of CO as COH or CHO which are precursor of methane. 3) The chemical state on the Cu electrode after CPE is promptly converted to Cu oxide from Cu^+. Other than the enhancement in generation of C_2 products, promotion of ethanol generation rather than ethylene is also interesting point. Similar results were reported by other groups, which is assumed to be due to the difference in intermediates and/or the increase in hydrogen adsorption originating from other elements or Cu^+ on Cu electrode[18)37)66)-68)]. In this study, as well, the formation of other elements, such as residual sulfur, and/or Cu^+ may affect the property of electrode, inducing ethanol production. Since the mechanism is adopted only when CPE is performed at a high negative potential, we should also consider the mechanism which occurs at low potential. Unfortunately, the low-potential mechanism cannot be proposed at this stage because the results of our experiments have not yet been interpreted in terms of DFT calculations. For example, accelerating adsorption of H and CO on Cu, which is induced by the methane thiol layer, is believed to promote C_2 production. As mentioned above, Liu *et al.* previously reported that sulfur on Cu promotes adsorption of H and CO on Cu in DFT calculations[58]. In an analytical investigation, Phillips *et al.* identified enhancement in adsorption of CO on Cu, as well[22]. From the results, we assume that adsorption of H and CO promotes generation of C_2 products. Luo *et al.* reported that adsorption of H on Cu promotes generation of ethanol from CO_2[68]. This observation is in good agreement with our results in CPE. Our DFT calculations are in progress, and we plan to provide clarification in a subsequent report.

Conclusion

In summary, we investigated the role of a heteroatom on a Cu electrode modified with methane thiol monolayers in electrochemical CO_2 reduction, which provides enhanced selectivity for C2 products than a bare Cu electrode. In order to evaluate the mechanism, we performed *in situ* ATR-SEIRAS, SEM, GIWAXS, and XPS. In these analyses, it is confirmed that a roughened Cu surface is formed under CPE, which is induced by reductive desorption of methane thiol at negative potential greater than −1.4 V vs. Ag/AgCl. DFT calculations were also carried out to indicate that roughened surface is favorable for generating C_2 products. In addition, formation of Cu^+ on Cu was also demonstrated by detection of the peak ascribed to CO adsorbed on Cu+ by *in situ* ATR-SEIRAS. These observations indicate that in addition to the roughened structure, the Cu^+ moiety promotes generation of C_2 products. We believe that these findings will contribute to the development of effective Cu catalysts with high selectivity for conversion of CO_2 to useful compounds via electrochemical reduction. For the effect of other types of R substituents, we are now trying to evaluate. In addition, the DFT calculations will also be performed for other ligands on Cu. These will be reported in near future.

References

1) Xiaoding, X.; Moulijn, J. A. Mitigation of CO_2 by Chemical Conversion: Plausible Chemical Reactions and Promising Products. *Energy Fuels* **1996**, *10*, 305–325.
2) Song, C. Global Challenges and Strategies for Control, Conversion and Utilization of CO_2 for Sustainable Development Involving Energy, Catalysis, Adsorption and Chemical Processing. *Catal. Today* **2006**, *115*, 2–32.
3) Kim J.; Johnson T. A.; Miller J. E.; Stecheld E. B.; Maravelias C. T. Fuel Production from CO_2 using Solar-Thermal Energy: System Level Analysis. *Energy Environ. Sci*. **2012**, *5*, 8417–8429.
4) Newman, J.; Hoertz, P. G.; Bonino, C. A.; Trainham, J. A. Review: An Economic Perspective on Liquid Solar Fuels. *J. Electrochem. Soc*. **2012**, *159*, A1722–A1729.
5) Qiao, J.; Liu, Y.; Hong, F.; Zhang, J. A Review of Catalysts for the Electroreduction of Carbon Dioxide to Produce Low-Carbon Fuels. *Chem. Soc. Rev*. **2014**, *43*, 631–675.
6) Hori, Y.; Kikuchi, K.; Suzuki, S. Production of CO and CH_4 in Electrochemical Reduction of CO_2 at Metal Electrodes in Aqueous Hydrogencarbonate Solution. *Chem. Lett*. **1985**, *14*, 1695–1698.
7) Hori, Y.; Takahashi, I.; Koga, O.; Hoshi, N. Selective Formation of C_2 Compounds from Electrochemical Reduction of CO_2 at a Series of Copper Single Crystal Electrodes. *J. Phys. Chem. B* **2002**, *106*, 15–17.
8) Ren, D.; Deng, Y. L.; Handoko, A. D.; Chen, C. S.; Malkhandi, S.; Yeo, B. S. Selective Electrochemical Reduction of Carbon Dioxide to Ethylene and Ethanol on Copper(I) Oxide Catalysts. *ACS Catal*. **2015**, *5*, 2814–2821.
9) Roberts, F. S.; Kuhl, K. P.; Nilsson, A. High Selectivity for Ethylene from Carbon Dioxide Reduction over Copper Nanocube Electrocatalysts. *Angew. Chem*. **2015**, *127*, 5268–5271.
10) Yang, K. D.; Ko, W. R.; Lee, J. H.; Kim, S. J.; Lee, H.; Lee, M. H.; Nam, K. T. Morphology-Directed Selective Production of Ethylene or Ethane from CO_2 on a Cu Mesopore Electrode. *Angew. Chem., Int. Ed*. **2017**, *56*, 796–800.
11) Klingan, K.; Kottakkat, T.; Jovanov, Z. P.; Jiang, S.; Pasquini, C.; Scholten, F.; Kubella, P.; Bergmann, A.; Cuenya, B. R.; Roth, C.; Dau, H. Reactivity Determinants in Electrodeposited Cu Foams for Electrochemical CO_2 Reduction. *ChemSusChem*. **2018**, *11*, 3449–3459.
12) Arán-Ais, R. M.; Scholten, F; Kunze, S; Rizo, R; Cuenya, B. R. The Role of In Situ Generated Morphological Motifs and Cu (I) Species in C_{2+} Product Selectivity during CO_2 Pulsed Electroreduction. *Nature Energy* **2020**, *5*, 317–325.
13) Jeong, H. M.; Kwon, Y.; Won. J. H.; Lum, Y.; Cheng, M.-J.; Kim, K. H.; Head-Gordon, M.; Kang, J. K. Atomic-Scale Spacing between Copper Facets for the Electrochemical Reduction of Carbon Dioxide. *Adv. Energy Mater*. **2020**, *10*, 1903423.
14) Liu, J.; Fu, J.; Zhou, Y.; Zhu, W.; Jiang, L.-P.; Lin, Y. Controlled Synthesis of EDTA-Modified Porous Hollow Copper Microspheres for High-Efficiency Conversion of CO_2 to Multicarbon Products. *Nano Lett*. **2020**, *20*, 4823–4828.
15) Zhuang, T.-T.; Pang, Y.; Liang, Z.-Q.; Wang, Z.; Li, Y.; Tan, C.-S.; Li, J.; Dinh, C. T.; Luna, P. D.; Hsieh, P.-L.; Burdyny, T.; Li, H.-H.; Liu, M.; Wang, Y.; Li, F.; Proppe, A.; Johnston, A.; Nam, D.-H.; Wu, Z.-Y.; Zheng, Y.-R.; Ip, A. H.; Tan, H.; Chen, L.-J.; Yu, S.-H.; Kelley, S. O.; Sinton, D.; Sargent, E. H. Copper Nanocavities Confine Intermediates for Efficient Electrosynthesis of C_3 Alcohol Fuels from Carbon Monoxide. *Nature Catal*. **2018**, *1*, 946–951.
16) Ren, D.; Deng, Y. L.; Handoko, A. D.; Chen, C. S.; Malkhandi, S.; Yeo, B. S. Selective Electrochemical Reduction of Carbon Dioxide to Ethylene and Ethanol on Copper(I) Oxide Catalysts. *ACS Catal*. **2015**, *5*, 2814–2821.
17) Liang, Z.-Q.; Zhuang, T.-T.; Seifitokaldani, A.; Li, J.; Huang, C.-W.; Tan, C.-S.; Li, Y.; De Luna, P.; Dinh, C.-T.; Hu, Y.; Xiao, Q.; Hsieh, P.-L.; Wang, Y.; Li, F.; Quintero-Bermudez, R.; Zhou, Y.; Chen, P.; Pang, Y.; Lo, S.-C.; Chen, L.-J.; Tan, H. A.; Tan, H.; Xu, Z.; Zhao, S.; Sinton, D.; Sargent, E. H. Copper-on-Nitride Enhances the Stable Electrosynthesis of Multi-Carbon Products from CO_2. *Nature Commun*. **2018**, *9*, 3828.
18) Ebaid, M.; Jiang, K.; Zhang, Z.; Drisdell, W. S.; Bell, A. T.; Cooper, J. K. Production of C_2/C_3 Oxygenates from Planar Copper Nitride-Derived Mesoporous Copper via Electrochemical Reduction of CO_2. *Chem. Mater*. **2020**, *32*, 3304–3311.
19) Zhuang, T.-T.; Liang, Z.-Q.; Seifitokaldani, A.; Li, Y.; De Luna, P.; Burdyny. T.; Che, F.; Meng, F.; Min, Y.; Quintero-Bermudez, R.; Dinh, C.-T.; Pang, Y.; Zhong, M.; Zhang, B.; Li, J.; Chen, P.-N.; Zheng, X.-L.; Liang, H.; Ge, W.-N.; Ye, B.-J.; Sinton, D.; Yu, S.-H.; Sargent, E. H. Steering Post C-C Coupling Selectivity Enables High Efficiency Electroreduction of Carbon Dioxide to Multi-Carbon Alcohols. *Nature Catal.* **2018**, *1*, 421–428.
20) García-Muelas, R.; Dattila, F.; Shinagawa, T.; Martín, A. J.; Pérez-Ramírez, J.; López, N. Origin of Selective Electroreduction of Carbon Dioxide to Formate by Chalcogen Modified Copper. *J. Phys. Chem. Lett*. **2018**, *9*, 7153–7159.
21) Deng, Y.; Huang, Y.; Ren, D.; Handoko, A. D.; She, Z. W.; Hirunsit, P.; Yeo, B. S. On the Role of Sulfur for the Selective Electrochemical Reduction of CO_2 to Formate on CuSx Catalysts. *ACS Appl. Mater. Interfaces* **2018**, *10*, 28572–28581.
22) Phillips, K. R.; Katayama, Y.; Hwang, J.; Shao-Horn, Y. Sulfide-Derived Copper for Electrochemical Conversion of CO_2 to Formic Acid. *J. Phy. Chem. Lett*. **2018**, *9*, 4407–4412.
23) Ma, W.; Xie, S.; Zhang, X.-G.; Sun, F.; Kang, J.; Jiang, Z.; Zhang, Q.; Wu, D.-Y.; Wang, Y. Promoting Electrocatalytic CO_2 Reduction to Formate via Sulfur-Boosting Water

特集

Activation on Indium Surfaces. *Nature Commun*. **2019**, *10*, 892–901.

24) Higgins, D.; Landers, A. T.; Ji, Y.; Nitopi, S.; Morales-Guio, C. G.; Wang, L.; Chan, K.; Hahn, C.; Jaramillo, T. F. Guiding Electrochemical Carbon Dioxide Reduction toward Carbonyl Using Copper Silver Thin Films with Interphase Miscibility. *ACS Energy Lett*. **2018**, *3*, 2947–2955.

25) Hoang, T. T. H.; Verma, S; Ma, S.; Fister, T. T.; Timoshenko, J.; Frenkel, A. I.; Kenis, P. J. A.; Gewirth, A. A. Nanoporous Copper-Silver Alloys by Additive-Controlled Electrodeposition for the Selective Electroreduction of CO_2 to Ethylene and Ethanol. *J. Am. Chem. Soc*. **2018**, *140*, 5791–5797.

26) Li, C. W.; Kanan, M. W. CO_2 Reduction at Low Overpotential on Cu Electrodes Resulting from the Reduction of Thick Cu_2O Films. *J. Am. Chem. Soc*. **2012**, *134*, 7231–7234.

27) Eilert, A.; Cavalca, F.; Roberts, F. S.; Osterwalder, J.; Liu, C.; Favaro, M.; Crumlin, E. J.; Ogasawara, H.; Friebel, D.; Pettersson, L. G. M.; Nilsson, A. Subsurface Oxygen in Oxide-Derived Copper Electrocatalysts for Carbon Dioxide Reduction. *J. Phys. Chem. Lett*. **2017**, *8*, 285–290.

28) Velasco-Velez, J.-J.; Mom, R. V.; Sandoval-Diaz, L.-E.; Falling, L. J.; Chuang, C.-H.; Gao, D.; Jones, T. E.; Zhu, Q.; Arrigo, R.; Cuenya, B. R.; Knop-Gericke, A.; Lunkenbein, T.; Schlögl, R. Revealing the Active Phase of Copper during the Electroreduction of CO_2 in Aqueous Electrolyte by Correlating In Situ X-ray Spectroscopy and In Situ Electron Microscopy. *ACS Energy Lett*. **2020**, *5*, 2106–2111.

29) Shah, A. H.; Wang, Y.; Hussain, S.; Akbar, M. B.; Woldu, A. R.; Zhangab, X.; He, T. New Aspects of C_2 Selectivity in Electrochemical CO_2 Reduction over Oxide-Derived Copper. *Phys. Chem. Chem. Phys*. **2020**, *22*, 2046–2053.

30) Iijima, G.; Inomata, T.; Yamaguchi, H.; Ito, M.; Masuda, H. Role of a Hydroxide Layer on Cu Electrodes in Electrochemical CO_2 Reduction. *ACS Catal*. **2019**, *9*, 6305–6319.

31) Feng, X. F.; Jiang, K. L.; Fan, S. S.; Kanan, M. W. A Direct Grain-Boundary-Activity Correlation for CO Electroreduction on Cu Nanoparticles. *ACS Cent. Sci*. **2016**, *2*, 169–174.

32) Mandal, L.; Yang, K. R.; Motapothula, M. R.; Ren, D.; Lobaccaro, P.; Patra, A.; Sherburne, M.; Batista, V. S.; Yeo, B. S.; Ager, J. W.; Martin, J.; Venkatesan, T. Investigating the Role of Copper Oxide in Electrochemical CO_2 Reduction in Real Time. *ACS Appl. Mater. Interfaces* **2018**, *10*, 8574–8584.

33) Lei, Q.; Zhu, H.; Song, K.; Wei, N.; Liu, L.; Zhang, D.; Yin, J.; Dong, X.; Yao, K.; Wang, N.; Li, X.; Davaasuren, B.; Wang, J.; Han, Y. Investigating the Origin of Enhanced C_{2+} Selectivity in Oxide-/Hydroxide-Derived Copper Electrodes during CO_2 Electroreduction. *J. Am. Chem. Soc*. **2020**, *142*, 4213–4222.

34) Zhang, B.; Zhang, J.; Hua, M.; Wan, Q.; Su, Z.; Tan, X.; Liu, L.; Zhang, F.; Chen, G.; Tan, D.; Cheng, X.; Han, B.; Zheng, L.; Mo, G. Highly Electrocatalytic Ethylene Production from CO_2 on Nanodefective Cu Nanosheets. *J. Am. Chem. Soc*. **2020**, *142*, 13606–13613.

35) Ma, Z.; Tsounis, C.; Kumar, P. V.; Han, Z.; Wong, R. J.; Toe, C. Y.; Zhou, S.; Bedford, N. M.; Thomsen, L.; Ng, Y. H.; Amal, R. Enhanced Electrochemical CO_2 Reduction of Cu@Cu_xO Nanoparticles Decorated on 3D Vertical Graphene with Intrinsic sp^3-type Defect. *Adv. Funct. Mater*. **2020**, *30*, 1910118.

36) Fu, W.; Liu, Z.; Wang, T.; Liang, J.; Duan, S.; Xie, L.; Han, J.; Li, Q. Promoting C_{2+} Production from Electrochemical CO_2 Reduction on Shape-Controlled Cuprous Oxide Nanocrystals with High-Index Facets. *ACS Sustainable Chem. Eng*. **2020**, *8*, 15223–15229.

37) Lin, S.-C.; Chang, C.-C.; Chiu, S.-Y.; Pai, H.-T.; Liao, T.-Y.; Hsu, C.-S.; Chiang, W.-H.; Tsai, M.-K.; Chen, H. M. Operando Time-Resolved X-ray Absorption Spectroscopy Reveals the Chemical Nature Enabling Highly Selective CO_2 Reduction. *Nature Commun*. **2020**, *11*, 3525.

38) Scott, S. B.; Hogg, T. V.; Landers, A. T.; Maagaard, T.; Bertheussen, E.; Lin, J. C.; Davis, R. C.; Beeman, J. W.; Higgins, D.; Drisdell, W. S.; Hahn, C.; Mehta, A.; Seger, B.; Jaramillo, T. F.; Chorkendorff, I. Absence of Oxidized Phases in Cu under CO Reduction Conditions. *ACS Energy Lett*. **2019**, *4*, 803–804.

39) Timoshenko, J.; Jeon, H. S.; Sinev, I.; Haase, F. T.; Herzog, A.; Cuenya, B. R. Linking the Evolution of Catalytic Properties and Structural Changes in Copper–Zinc Nanocatalysts using Operando EXAFS and Neural-Networks. *Chem. Sci*. **2020**, *11*, 3727–3736.

40) Osawa, M. Dynamic Processes in Electrochemical Reactions Studied by Surface-Enhanced Infrared Absorption Spectroscopy (SEIRAS). *Bull. Chem. Soc. Jpn*. **1997**, *70*, 2861–2880.

41) Kuwabata, S.; Kanemoto, H.; Oyamatsu, D.; Yoneyama, H. Partial Desorption of Alkanethiol Monolayer from Gold Substrate Modified with Ag and Cu. *Electrochemistry* **1999**, *67*, 1254–1257.

42) Caprioli, F.; Martinelli, A.; Gazzoli, D.; Castro, V. D.; Decker, F. Enhanced Protective Properties and Structural Order of Self-Assembled Monolayers of Aromatic Thiols on Copper in Contact with Acidic Aqueous Solution. *J. Phys. Chem. C* **2012**, *116*, 4628–4636.

43) Huang, Y.; Handoko, A. D.; Hirunsit, P.; Yeo, B. S. Electrochemical Reduction of CO_2 Using Copper Single-Crystal Surface: Effects of CO_2 Coverage on the Selective Formation of Ethylene. *ACS Catal*. **2017**, *7*, 1749–1756.

44) Lee, S. Y.; Jung, H.; Kim, N.-K.; Oh, H.-S.; Min, B. K.; Hwang, Y. J. Mixed Copper States in Anodized Cu Electrocatalyst for Stable and Selective Ethylene Production from CO_2 Reduction. *J. Am. Chem. Soc*. **2018**, *140*, 8681–8689.

45) Gunathunge, C. M.; Ovalle, V. J.; Li, Y.; Janik, M. J.; Waegele, M. M. Existence of an Electrochemically Inert CO Population on Cu Electrodes in Alkaline pH. *ACS Catal.* **2018**, *8*, 7507–7516.

46) Giannozzi, P.; Baroni, S.; Bonini, N.; Calandra, M.; Car, R.; Cavazzoni, C.; Ceresoli, D.; Chiarotti, G. L.; Cococcioni, M.; Dabo, I.; Corso, A. D.; de Gironcoli, S.; Fabris, S.; Fratesi, G.; Gebauer, R.; Gerstmann, U.; Gougoussis, C.; Kokalj, A.; Lazzeri, M.; Martin-Samos, L.; Marzari, N.; Mauri, F.; Mazzarello, R.; Paolini, S.; Pasquarello, A.; Paulatto, L.; Sbraccia, C.; Scandolo, S.; Sclauzero, G.; Seitsonen, A. P.; Smogunov, A.; Umari, P.; Wentzcovitch, R. M. QUANTUM ESPRESSO: a Modular and Open-Source Software Project for Quantum Simulations of Materials. *J. Phys. Condens. Matter* **2009**, *21*, 395502.

47) Otani, M.; Sugino, O. First-Principles Calculations of Charged Surfaces and Interfaces: A Plane-Wave Nonrepeated Slab Approach. *Phys. Rev. B* **2006**, *73*, 115407.

48) Hamada, I.; Sugino, O.; Bonnet, N.; Otani M. Improved Modeling of Electrified Interfaces using the Effective Screening Medium Method. *Phys. Rev. B* **2013**, *88*, 155427.

49) Kovalenko, A.; Hirata, F. Three-Dimensional Density Profiles of Water in Contact with a Solute of Arbitrary Shape: a RISM Approach. *Chem. Phys. Lett.* **1998**, *290*, 237–244.

50) Nishihara, S.; Otani, M. Hybrid Solvation Models for Bulk, Interface, and Membrane: Reference Interaction Site Methods Coupled with Density Functional Theory. *Phys. Rev. B* **2017**, *96*, 115429.

51) Haruyama, J.; Ikeshoji, T.; Otani, M. Electrode Potential from Density Functional Theory Calculations Combined with Implicit Solvation Theory. *Phys. Rev. Materials* **2018**, *2*, 095801.

52) Yoshimoto, S.; Ono, Y.; Kuwahara, Y.; Nishiyama, K.; Taniguchi, I. *J. Phys. Chem. C* **2016**, *120*, 15803–15813.

53) Raciti, D.; Cao, L.; Livi, K. J. T.; Rottmann, P. F.; Tang, X.; Li, C.; Hicks, Z.; Bowen, K. H.; Hemker, K. J.; Mueller, T.; Wang, C. Low-Overpotential Electroreduction of Carbon Monoxide Using Copper Nanowires. *ACS Catal.* **2017**, *7*, 4467–4472.

54) Heyes, J.; Dunwell, M.; Xu, B. CO_2 Reduction on Cu at Low Overpotentials with Surface-Enhanced In Situ Spectroscopy. *J. Phys. Chem. C* **2016**, *120*, 17334–17341.

55) Malkani, A. S.; Dunwell, M.; Xu, B. Operand Spectroscopic Investigations of Copper and Oxide-Derived Copper Catalysts for Electrochemical CO Reduction. *ACS Catal.* **2019**, *9*, 474–478.

56) Gunathunge, C. M.; Li, J.; Li, X.; Hong, J. J.; Waegele, M. M. Revealing the Predominant Surface Facets of Rough Cu Electrodes under Electrochemical Conditions. *ACS Catal.* **2020**, *10*, 6908–6923.

57) Ayemoba, O.; Cuesta, A.; Spectroscopic Evidence of Size-Dependent Buffering of Interfacial pH by Cation Hydrolysis during CO_2 Electroreduction. *ACS Appl. Mater. Interfaces* **2017**, *9*, 27377–27382.

58) Liu, D.; Liu, Y.; Li, M. Understanding How Atomic Sulfur Controls the Selectivity of the Electroreduction of CO_2 to Formic Acid on Metallic Cu Surfaces. *J. Phys. Chem. C* **2020**, *124*, 6145–6153.

59) Luo, W.; Nie, X.; Janik, M. J.; Asthagiri, A. Facet Dependence of CO_2 Reduction Paths on Cu Electrodes. *ACS Catal.* **2016**, *6*, 219–229.

60) Xiao, H.; Cheng, T.; Goddard III, W. A. Atomistic Mechanisms Underlying Selectivities in C_1 and C_2 Products from Electrochemical Reduction of CO on Cu(111). *J. Am. Chem. Soc.* **2017**, *139*, 130–136.

61) Cheng, T.; Xiao, H.; Goddard III, W. A. Full Atomistic Reaction Mechanism with Kinetics for CO Reduction on Cu(100) from Ab Initio Molecular Dynamics Free-Energy Calculations at 298 K. *Proc. Natl. Acad. Sci. U. S. A.* **2017**, *114*, 1795–1800.

62) Liu, X.; Schlexer, P.; Xiao, J.; Ji, Y.; Wang, L.; Sandberg, R. B.; Tang, M.; Brown, K. S.; Peng, H.; Ringe, S.; Hahn, C.; Jaramillo, T. F.; Nørskov, J. K.; Chan, K. pH Effects on the Electrochemical Reduction of CO_2 towards C_2 Products on Stepped Copper. *Nature Commun.* **2019**, *10*, 32.

63) Schreier, M.; Yoon, Y.; Jackson, M. N.; Surendranath, Y. Competition between H and CO for Active Sites Governs Copper-Mediated Electrosynthesis of Hydrocarbon Fuels. *Angew. Chem. Int. Ed.* **2018**, *57*, 1 – 6.

64) Liu, X.; Xiao, J.; Peng, H.; Hong, X.; Chan, K.; Nørskov, J. K. Understanding Trends in Electrochemical Carbon Dioxide Reduction Rates. *Nature Commun.* **2017**, *8*, 15438.

65) Xiao, H.; Goddard III, W. A.; Cheng, T.; Liu, Y. Cu Metal Embedded in Oxidized Matrix Catalyst to Promote CO_2 Activation and CO Dimerization for Electrochemical Reduction of CO_2. *Proc. Natl. Acad. Sci. U. S. A.* **2017**, *114*, 6685–6688.

66) Li, Y. C.; Wang, Z.; Yuan, T.; Nam, D.-H.; Luo, M.; Wicks, J.; Chen, B.; Li, J.; Li, F.; García de Arquer, F. P.; Wang, Y.; Dinh, C.-T.; Voznyy, O.; Sinton, D.; Sargent, E. H. Binding Site Diversity Promotes CO_2 Electroreduction to Ethanol. *J. Am. Chem. Soc.* **2019**, *141*, 8584–8591.

67) Chen, Z.; Wang, T.; Liu, B.; Cheng, D.; Hu, C.; Zhang, G.; Zhu, W.; Wang, H.; Zhao, Z.-J.; Gong, J. Grain-Boundary-Rich Copper for Efficient Solar-Driven Electrochemical CO_2 Reduction to Ethylene and Ethanol. *J. Am. Chem. Soc.* **2020**, *142*, 6878–6883.

68) Luo, M.; Wang, Z.; Li, Y. C.; Li, J.; Li, F.; Lum, Y.; Nam, D.-H.; Chen, B.; Wicks, J.; Xu, A.; Zhuang, T.; Leow, W. R.; Wang, X.; Dinh, C.-T.; Wang, Y.; Wang, Y.; Sinton, D.; Sargent, E. H. Hydroxide Promotes Carbon Dioxide Electroreduction to Ethanol on Copper via Tuning of Adsorbed Hydrogen. *Nature Commun.* **2019**, *10*, 5814.

特集

著者

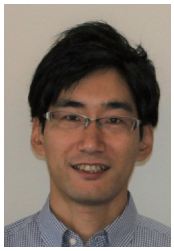

飯島 剛
いいじま ごう

マテリアル研究部
電気化学材料の開発に従事

世登 裕明
よとう ひろあき

マテリアル研究部　博士（工学）
材料要素技術開発に従事

山口 仁
やまぐち ひとし

マテリアル研究部　博士（工学）
第一原理等の理論計算に従事

伊藤 みほ
いとう みほ

先端技術研究所　博士（工学）
先端技術研究に従事

猪股 智彦
いのまた ともひこ

名古屋工業大学大学院　工学研究科工学専攻　准教授　理学博士
分子修飾による機能性材料の研究に従事

増田 秀樹
ますだ ひでき

名古屋工業大学　名誉教授・プロジェクト教授
愛知工業大学工学研究科　客員教授
薬学博士
生体関連小分子の捕捉・活性化の研究に従事